Rate of magnetization reversal due to nucleation of soliton-antisoliton pairs at point-like defects

Peter N. Loxley
School of Physics, The University of Sydney, New South Wales 2006, Australia
(Received 10 October 2007; revised manuscript received 31 March 2008; published 23 April 2008)

The rate of magnetization reversal due to the nucleation of soliton-antisoliton pairs at point-like defects is found for a uniaxial ferromagnet in an applied magnetic field. Point-like defects are considered as local variations in the magnetic anisotropy over a length scale smaller than the domain-wall width. A weak magnetic field applied along the easy axis causes the magnetization to become metastable, and the lowest activation barrier for reversal involves the nucleation of a soliton-antisoliton pair pinned to a point-like defect. Formulas are derived for the activation energy and field of reversal, and the reversal-rate prefactor is calculated using Langer's theory for the decay of a metastable state. As the applied field tends to zero, the lowest activation energy is found to be exactly half that of an unpinned soliton-antisoliton pair, and results from the formation of a spatially nonuniform metastable state when the defect strength become large. The smallest field of reversal is exactly half of the anisotropy field. The reversal-rate prefactor is found to increase with the number of point-like defects but decreases with increase in the defect strength due to a decrease in the activation entropy when translational symmetry is broken by the point-like defects, and soliton-antisoliton pairs become more strongly localized to the pinning sites.

DOI: 10.1103/PhysRevB.77.144424 PACS number(s): 75.60.Jk, 64.60.Q−, 64.60.My, 05.45.Yv

I. INTRODUCTION

Thermal stability and the decay of metastable states have been widely studied since the pioneering work of Van't Hoff and Arrhenius.[1] Detailed theories of thermally activated magnetization reversal were originally proposed for single-domain ferromagnetic particles.[2,3] However, recent interest in multidomain ferromagnets such as elongated particles and nanowires, exchange springs, and coupled magnetic grains has led to new theories and new predictions for rates of thermally activated reversal.[4–8]

During the reversal of a single-domain ferromagnetic particle, the magnetization is assumed to rotate coherently. This is no longer true for effectively one-dimensional (1D) ferromagnets, where reversal can take place via the nucleation of soliton-antisoliton pairs.[4,5] This typically takes place as follows: Initially, the magnetization is uniformly aligned along a particular anisotropy axis but becomes metastable when a weak magnetic field is applied in the opposite direction to the magnetization, that is, it remains stable to small thermal fluctuations which occur frequently but becomes unstable to the less frequent larger fluctuations. The magnetic anisotropy is generally sufficient to stabilize the magnetization when small fluctuations are present. However, a large fluctuation may create a region of partially reversed magnetization which forms a *nucleus of critical size*. Following the formation of a nucleus of critical size given by a soliton-antisoliton pair, the soliton and antisoliton are driven apart by the applied field, and the magnetization reverses direction. Solitons as fundamental excitations in 1D magnets is not a new concept, and much work has previously been done on soliton statistical mechanics and nonlinear dynamics following the work of Bloch, Döring, Enz, and Walker.[9–14] However, recent experimental progress in the preparation and characterization of ferromagnetic nanowires,[15–19] including multilayered nanowires and nanowires with controlled defects, has generated particular interest in the reversal mechanisms and switching rates of 1D magnetic systems.[4–7,20–26]

In many realistic situations, it is known that nucleation occurs at a nonuniformity or defect—such as an irregularity in a sample. Such defects supposedly lower the activation energy for nucleation, allowing it to occur more frequently. In magnetic systems, defects may include nonuniformities in the magnetic anisotropy and exchange,[6,7] or local deviations from an otherwise uniform geometry.[27] Reversal due to nucleation at defects presents some conceptual difficulties. For example, a defect which lowers the activation energy for nucleation usually favors domain-wall pinning over domain-wall propagation: the opposite of what is required for reversal to take place. How defects modify the nucleus of critical size and the metastable state is also largely unknown. Another consideration is the probability of nucleation at a defect. There are usually far fewer nucleation sites available for nucleation at a defect than for nucleation elsewhere in a sample.

The purpose of this paper is to carry out a theoretical investigation of thermally activated magnetization reversal due to nucleation at defects. The type of defects considered includes local variations in the magnetic anisotropy over a length scale smaller than the domain-wall width—so-called point-like defects. Activated reversal due to defects larger than the domain-wall width has previously been treated in Refs. 6 and 7. A general model of a 1D uniaxial ferromagnet in an applied magnetic field is employed to calculate the rate of reversal using Langer's theory for the rate of decay of a metastable state.[28,29] Although 1D magnetic systems are specifically treated, the model is general enough to include other 1D systems which obey a time-independent double sine-Gordon equation.

The rate of thermally activated reversal can be described using the well-known Van't Hoff–Arrhenius law:

$$I = I_0 e^{-\beta E_a}, \tag{1}$$

where E_a is the activation energy, and is given by the height of the lowest energy barrier separating a metastable magne-

tization state from the fully reversed state, $\beta=1/k_BT$, and I_0 is the reversal-rate prefactor and depends on the dynamics of crossing the activation barrier, as well as on the *activation entropy*—the entropy difference between the activated and metastable states.[1] The exponential in Eq. (1) implies thermal activation takes place over a much larger time scale than the time scales in I_0 characterizing the magnetization dynamics.

Previous theories for nucleation at point-like defects have concentrated on calculating E_a using the sine-Gordon model,[30] and E_a and I_0 using a reaction-diffusion equation with piecewise-linear nonlinearity.[31] Neither of these treatments is adequate for addressing the questions posed here. The first treatment does not attempt to find I_0, and neither treatment considers the double sine-Gordon model—which is necessary for describing a ferromagnet in an applied magnetic field. In this work, mathematical analysis is used to derive expressions for E_a and I_0 for a 1D uniaxial ferromagnet in an applied magnetic field.

The structure of this paper consists of two parts. In Secs. II and III, the model is introduced, and a reversal mechanism is proposed from consideration of the minima and saddle points of the relevant energy function. A critical defect strength is identified—above which the metastable state may become spatially nonuniform—and formulas are derived for E_a and the field of reversal H_{rev} above and below the critical defect strength. In Sec. IV, a formula is derived for I_0 below the critical defect strength as the applied field tends to zero. This allows for a reasonably straightforward understanding of how the presence of point-like defects can modify I_0. A summary and discussion of the main results is given in Sec. V.

II. MODEL

The magnetization is described by the unit vector $\boldsymbol{m}$, and the energy of magnetic configurations of a 1D uniaxial ferromagnet of length L, and cross-section area $\mathcal{A}_r$, is assumed to have the form

$$E=\mathcal{A}_r\int_{-L/2}^{L/2}dx\left[A\left(\frac{\partial \boldsymbol{m}}{\partial x}\right)^2-K(x)m_x^2-\mu_0M_sHm_x\right]. \quad (2)$$

The first term in Eq. (2) follows from the classical-continuum limit of the exchange interaction between neighboring spins in the Heisenberg Hamiltonian, while the second and third terms describe the magnetic anisotropy and Zeeman energies due to an easy axis along the x axis and a magnetic field applied along the easy axis, respectively.[13,14,32] The first term energetically favors uniform magnetization, the second term favors magnetization which points in either direction along the easy axis, while the last term breaks this symmetry so that one direction is favored over the other.

A key assumption in applying Eq. (2) to ferromagnetic materials is that the magnetization varies only along the longitudinal direction of a sample, and any transverse variation is assumed to be negligible. This 1D approximation is expected to hold whenever the transverse length is less than

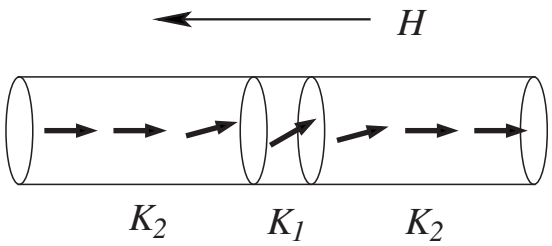

FIG. 1. A 1D uniaxial ferromagnet resulting from a cylindrical geometry with $d<\pi\delta_{\text{ex}}$. The easy axis lies along the longitudinal axis, and a magnetic field is applied along the easy axis. A point-like defect represents a local reduction in the strength of magnetic anisotropy ($K_1<K_2$), or a local misalignment in the anisotropy direction ($K_1<0$). The sequence of arrows represents a metastable magnetization state.

$\pi\delta_{\text{ex}}$, where $\delta_{\text{ex}}=\sqrt{A/\mu_0M_s^2}$ is the magnetic exchange length.[5] Below this critical length, the cost in exchange energy for $\boldsymbol{m}$ to deviate from a uniform configuration outweighs the possible reduction in energy from the demagnetizing field. One possibility for a 1D uniaxial ferromagnet therefore consists of a cylindrical geometry with $d<\pi\delta_{\text{ex}}$, as shown in Fig. 1. Values of $\pi\delta_{\text{ex}}$ range between 5 and 10 nm for common ferromagnetic materials such as Co, Ni, and Fe.[32]

Defects in the magnetic anisotropy are taken into account by allowing $K(x)$ in Eq. (2) to vary with x. If L_d is the defect width, a point-like defect is assumed to satisfy $L_d<\pi\delta_w$, where $\pi\delta_w$ is the characteristic domain-wall width. Provided that exchange coupling extends over the defect region, a point-like defect located at $x=0$ can be approximated using

$$K(x)=K-\Delta KL_d\delta(x), \quad (3)$$

where $\Delta K\geqslant 0$ is the change in K due to the defect and $\delta(x)$ is the Dirac delta function. In Fig. 1, $K=K_2$ and $\Delta K=K_2-K_1$ has been assumed. A defect leading to a reduction in the strength of magnetic anisotropy will satisfy $K_1<K_2$, while a defect corresponding to a local misalignment in the anisotropy direction may have $K_1<0$. The anisotropy constants include both crystalline and local magnetostatic effects.[5]

The magnetization is assumed to undergo dissipative dynamics according to the Landau-Lifshitz equation:

$$\frac{\partial \boldsymbol{M}}{\partial t}=-\gamma\boldsymbol{M}\times\boldsymbol{H}_{\text{eff}}-\frac{\Lambda\gamma}{M_s}\boldsymbol{M}\times(\boldsymbol{M}\times\boldsymbol{H}_{\text{eff}}), \quad (4)$$

where $\boldsymbol{M}=M_s\boldsymbol{m}$, γ is the gyromagnetic ratio, and Λ is a dimensionless damping parameter.[13,14,32] The first term in Eq. (4) describes precession of the magnetization in an effective magnetic field given by $\boldsymbol{H}_{\text{eff}}=-\delta E/\delta\boldsymbol{M}$ and conserves the energy. The second term is nonconservative and describes the relaxation of $\boldsymbol{M}$ toward $\boldsymbol{H}_{\text{eff}}$ due to energy dissipation. The effect of thermal fluctuations could also be included in Eq. (4) by adding an additional term to represent stochastic forces acting on the magnetization.[4] Here, however, thermal fluctuations will be treated using the methods of statistical mechanics, as shown in Appendix A.

The length, energy, and time scales of interest are the width $\pi\delta_w$ and energy $2\Delta_w$ of a domain wall outside the

defect region and the characteristic time τ of magnetization precession in the anisotropy field outside the defect region, where

$$\delta_w = \sqrt{\frac{A}{K}}, \quad \Delta_w = 2\mathcal{A}_r\sqrt{AK}, \quad \tau = \frac{M_s}{2\gamma K}. \tag{5}$$

The magnitude $|\boldsymbol{m}|$ is conserved by Eq. (4), and the magnetization is most conveniently expressed in spherical-polar coordinates as $\boldsymbol{m}=(\sin\theta\cos\phi, \sin\theta\sin\phi, \cos\theta)$. In terms of spherical-polar coordinates and the characteristic length and energy scales defined in Eq. (5), the energy expression given by Eq. (2) becomes

$$E = \int_{-L/2}^{L/2} dx \left[\frac{1}{2}\left\{ \left(\frac{\partial\theta}{\partial x}\right)^2 + \sin^2\theta\left(\frac{\partial\phi}{\partial x}\right)^2 \right\} + V - \alpha\delta(x)V_d \right], \tag{6}$$

where

$$V = V_d - h\sin\theta\cos\phi, \quad V_d = -\frac{1}{2}\sin^2\theta\cos^2\phi, \tag{7}$$

and where a dimensionless defect strength α and a dimensionless applied field h have been defined as

$$\alpha = \frac{L_d\Delta K}{\delta_w K} \tag{8}$$

and

$$h = \frac{\mu_0 M_s H}{2K}. \tag{9}$$

III. REVERSAL MECHANISM AND ACTIVATION ENERGY

Mechanisms for thermally activated magnetization reversal involve configurations which are the minima and saddle points of Eq. (6). Local minima of Eq. (6) become metastable at nonzero temperature due to thermal fluctuations, and magnetization reversal involves crossing over the lowest saddle point in Eq. (6) separating a local minimum from the global minimum. Following the identification of a critical defect strength, a reversal mechanism is proposed, and the corresponding activation energy and field of reversal are found.

A. Energy minima and saddle points

Configurations which are minima, maxima, or saddle points of Eq. (6) solve the corresponding Euler-Lagrange equations. The Euler-Lagrange equation for θ is solved by $\theta=\pi/2$, and the Euler-Lagrange equation for ϕ then becomes

$$-\frac{d^2\phi}{dx^2} + V'(\phi) - \alpha\delta(x)V_d'(\phi) = 0, \tag{10}$$

where $V(\phi)=-1/2\cos^2\phi - h\cos\phi$ and $V_d(\phi)=-1/2\cos^2\phi$. When $\alpha=0$, Eq. (10) reduces to the time-independent double sine-Gordon equation, and spatially uniform configurations satisfy $V'(\phi)=0$. When $h=0$, two of the degenerate minima of $V(\phi)$ are given by $\phi=0$ and $\phi=\pi$ and correspond to the magnetization pointing in either direction along the easy axis. When $h>0$, the degeneracy is broken, and the minimum at $\phi=\pi$ becomes metastable at nonzero temperature—thermal fluctuations eventually lead the system to the lower energy minimum at $\phi=0$.

Spatially nonuniform configurations can be found for $\alpha=0$ by integrating Eq. (10) once using the integrating factor $d\phi/dx$ to yield

$$\frac{1}{2}\left(\frac{d\phi}{dx}\right)^2 - V(\phi) = C, \tag{11}$$

where C is an arbitrary constant of integration. In the limit as $L\to\infty$, integrating Eq. (11) with $C=1/2-h$ yields a bound soliton-antisoliton pair (see Ref. 33):

$$\phi_{\text{sap}} = \phi_s\left(\frac{x-x_0}{\delta_s} - R\right) + \phi_s\left(-\frac{x-x_0}{\delta_s} - R\right), \tag{12}$$

where $\phi_s(y)=2\arctan e^y$ represents a single soliton, $\phi_s(-y)$ represents an antisoliton, and

$$\delta_s = \frac{1}{\sqrt{1-h}}, \quad \operatorname{sech}^2 R = h. \tag{13}$$

The parameter $2R$ gives the distance separating the soliton and antisoliton as $h\to 0$, while x_0 is the position of the "center of mass" of the soliton-antisoliton pair. The value of x_0 is arbitrary in a uniform system due to the underlying translational symmetry, while R is fixed by the applied field according to Eq. (13). In any sequence of configurations which transform $\phi=\pi$ into $\phi=0$, the soliton-antisoliton pair has the maximum energy. Relative to $\phi=\pi$, this energy is given by

$$E_{\text{sap}} = 4\sqrt{1-h} - 4h\,\operatorname{arcsech}(\sqrt{h}). \tag{14}$$

For the biaxial ferromagnet considered in Ref. 4, Eq. (14) represents the activation energy for reversal when no defects are present.

Inclusion of a point-like defect implies $\alpha\neq 0$ in Eq. (10). Integrating this equation from $-\varepsilon$ to ε, and letting $\varepsilon\to 0$, yields the following consistency condition:

$$\left.\frac{d\phi}{dx}\right|_{x=0^+} - \left.\frac{d\phi}{dx}\right|_{x=0^-} = -\alpha V_d'(\phi)|_{x=0}. \tag{15}$$

The simplest configuration satisfying Eq. (15) has a continuous first derivative everywhere, and Eq. (15) reduces to $V_d'(\phi)=0$ at $x=0$. Upon using V_d from Eq. (7), the nontrivial pinning solution is given by $\phi=\pi/2$ at $x=0$. The solution given by Eq. (12) can be made to satisfy this by choosing x_0 to be

$$\frac{x_0}{\delta_s} = \pm\,\operatorname{arccosh}\left(\sqrt{\frac{1-h}{h}}\right). \tag{16}$$

The configuration given by Eqs. (12) and (16) describes a *pinned soliton-antisoliton pair*: a soliton-antisoliton pair with either the soliton or the antisoliton centered at $x=0$. This

solution is valid for $0 \leqslant h \leqslant 1/2$. The energy can be found using Eqs. (6), (12), and (16) and relative to $\phi=\pi$ is given by

$$E_{\mathrm{pin}} = E_{\mathrm{sap}} - \alpha/2. \tag{17}$$

The types of defect considered here satisfy $\alpha>0$, so $E_{\mathrm{pin}} < E_{\mathrm{sap}}$, and the energy of a soliton-antisoliton pair decreases when it becomes pinned to a point-like defect.

The simplest configuration satisfying Eq. (15) with a discontinuous first derivative is one that is symmetric at the pinning site: $\phi(-x)=\phi(x)$. Such a configuration can be constructed as

$$\phi = \begin{cases} \phi_{\mathrm{sap}}(x+x_0), & x>0 \\ \phi_{\mathrm{sap}}(x-x_0), & x<0, \end{cases} \tag{18}$$

where $\phi_{\mathrm{sap}}(x-x_0)$ is given by Eq. (12) and $\phi_{\mathrm{sap}}(x+x_0)$ has the same form as Eq. (12), but with x_0 of the opposite sign. For this configuration, Eq. (15) becomes $2d\phi/dx = \pm \alpha V_d'(\phi)$ at $x=0$. To write $d\phi/dx$ in terms of ϕ_{sap}, the first integral given by Eq. (11) and the boundary conditions satisfied by Eq. (12) are used, yielding $(d\phi_{\mathrm{sap}}/dx)^2 = 2V(\phi_{\mathrm{sap}}) + 1 - 2h$. Upon using this and the expressions for V and V_d, Eq. (15) can be written as $F(\cos\phi_0)=0$, where

$$F(m) \equiv \left[(1-m)\left(1-\frac{\alpha}{2}m\right)\left(1+\frac{\alpha}{2}m\right) - 2h\right][1+m], \tag{19}$$

and $\phi_0 \equiv \phi(x=0)$ depends on the value of x_0. This equation has four possible solutions for $\cos\phi_0$, each one corresponding to a different configuration of Eq. (18). The $\phi=\pi$ state is given by the $\cos\phi_0=-1$ solution which always satisfies this equation (a different choice of boundary conditions will yield a solution for the $\phi=0$ state). Classifying the behavior of Eq. (19) at $m=-1$ allows critical values of the applied field and defect strength to be identified. Specifically, at $m=-1$, $F'(m)=0$ when $h=h_{\mathrm{crit}}$ and $F''(m)=0$ when $\alpha=\alpha_{\mathrm{crit}}$, where

$$h_{\mathrm{crit}} = 1 - \left(\frac{\alpha}{2}\right)^2, \quad \alpha_{\mathrm{crit}} = 2/\sqrt{5} \simeq 0.89. \tag{20}$$

These critical values allow the metastable state to be properly quantified. It will be shown that $\phi=\pi$ becomes unstable when $h=h_{\mathrm{crit}}$. If $\alpha<\alpha_{\mathrm{crit}}$, it then decays into the fully reversed state $\phi=0$. However, if $\alpha>\alpha_{\mathrm{crit}}$, it will be shown that $\phi=\pi$ decays into a new metastable state which is *spatially nonuniform*. A mechanism for reversal is now proposed.

B. Reversal mechanism for $\alpha<\alpha_{\mathrm{crit}}$

In the absence of defects, reversal of a 1D ferromagnet involves the nucleation of a soliton-antisoliton pair from a uniform metastable state,[4] as outlined in Sec. I. However, the presence of one or more point-like defects leads to a saddle-point configuration of lower energy. When $h \leqslant 1/2$, this is given by the pinned soliton-antisoliton pair from Eqs. (12) and (16). Upon reintroducing units into Eq. (17), the energy required to nucleate a pinned soliton-antisoliton pair becomes

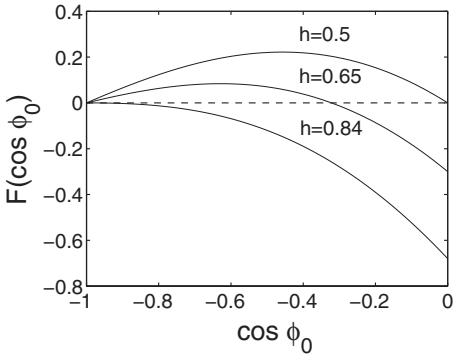

FIG. 2. Graphical solution of $F(\cos\phi_0)=0$ for $\alpha<\alpha_{\mathrm{crit}}$. When $\alpha=0.8$, the left-hand side of Eq. (19) (solid) intersects zero (dashed) twice between $-1 \leqslant \cos\phi_0 \leqslant 0$ for $0.5 \leqslant h < 0.84$.

$$\Delta E_{\mathrm{nuc}} = 2\mathcal{A}_r\sqrt{AK}E_{\mathrm{pin}}. \tag{21}$$

This energy reaches a maximum value $\Delta E_{\mathrm{nuc}}=8\mathcal{A}_r\sqrt{AK}$ as $h\to 0$ and $\alpha\to 0$, which is the energy of two domain walls.[32] When $\alpha=\alpha_{\mathrm{crit}}$ and $h=1/2$, Eq. (21) reaches its minimum value: $\Delta E_{\mathrm{nuc}} \simeq 1.24\mathcal{A}_r\sqrt{AK}$, which is less than one-third the energy of one domain wall.[32]

Following the nucleation of a soliton-antisoliton pair, reversal takes place when the pair moves apart under the action of the applied field. However, it will be shown in Sec. IV B that one member of the pair remains pinned to a point-like defect if $h<\alpha/2$. In this case, a soliton must become unpinned before reversal can be completed. From Eq. (2), the maximum energy to unpin a soliton is $\Delta E_{\mathrm{dp}}=\mathcal{A}_r\Delta K L_d$ at zero applied field and results from the sudden increase in anisotropy at the center of the soliton when it is moved away from the defect region. When the applied field is nonzero, ΔE_{dp} will decrease due to the Zeeman energy contribution. Written in terms of α, this implies

$$\Delta E_{\mathrm{dp}} \leqslant \mathcal{A}_r\sqrt{AK}\alpha. \tag{22}$$

Comparing Eqs. (21) and (22), it is seen that $\Delta E_{\mathrm{nuc}} > \Delta E_{\mathrm{dp}}$ when $\alpha<\alpha_{\mathrm{crit}}$, so nucleation provides the rate-determining step for reversal. The activation energy for reversal is therefore given by

$$E_a = \Delta E_{\mathrm{nuc}}. \tag{23}$$

At $h=1/2$, there is a smooth transition from the saddle-point configuration given by the pinned soliton-antisoliton pair in Eqs. (12) and (16) to one given by Eq. (18) with $\phi_0=\pi/2$. A graphical solution of $F(\cos\phi_0)=0$ for $\alpha<\alpha_{\mathrm{crit}}$ and $h \leqslant h_{\mathrm{crit}}$ is given in Fig. 2. At $h=1/2$, the $\phi_0=\pi/2$ solution corresponds to the rightmost intersection of the solid curve with the dashed line in Fig. 2. When $h>1/2$, this intersection moves toward the intersection at $\cos\phi_0=-1$, until they eventually coalesce at $h_{\mathrm{crit}}=0.84$ when the slope of the solid curve goes to zero at $\cos\phi_0=-1$. In this case, the saddle-point configuration has merged with the $\phi=\pi$ metastable state, which subsequently becomes unstable. The activation energy for reversal then vanishes, and reversal takes place spontaneously. After reintroducing units, the field of reversal is given by

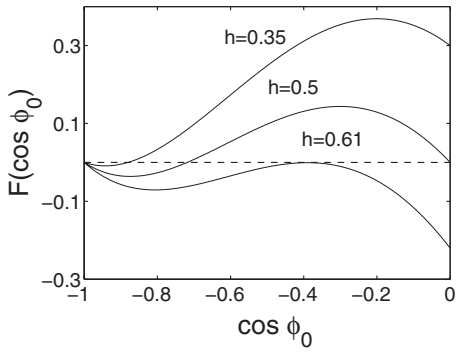

FIG. 3. Graphical solution of $F(\cos\phi_0)=0$ for $\alpha>\alpha_{\rm crit}$. When $\alpha=1.8$, the left-hand side of Eq. (19) (solid) intersects zero (dashed) three times between $-1\leqslant\cos\phi_0\leqslant 0$ for $0.5\leqslant h<0.61$.

$$H_{\rm rev}=\frac{2K}{\mu_0 M_s}h_{\rm crit}. \tag{24}$$

When $\alpha=0$, Eq. (24) reaches its maximum value $H_{\rm rev}=2K/\mu_0 M_s$, which is just the anisotropy field,[32] corresponding to the field of reversal when no defects are present. When $\alpha=\alpha_{\rm crit}$, Eq. (24) yields $H_{\rm rev}=1.6K/\mu_0 M_s$, which is exactly 0.8 of the anisotropy field.

C. Reversal mechanism for $\alpha>\alpha_{\rm crit}$

When $\alpha<\alpha_{\rm crit}$, the uniform metastable state becomes unstable as the saddle-point configuration merges with $\phi=\pi$ at $h=h_{\rm crit}$. This is no longer possible when $\alpha>\alpha_{\rm crit}$, and the uniform metastable state becomes unstable only after a nonuniform metastable state has been created. A graphical solution of $F(\cos\phi_0)=0$ for $\alpha>\alpha_{\rm crit}$ and $h>h_{\rm crit}$ is shown in Fig. 3. When $h=0.35$, there are two intersections in Fig. 3 as the local minimum moves away from $\cos\phi_0=-1$, corresponding to two solutions of $F(\cos\phi_0)=0$. When $h=1/2$, there are three intersections in Fig. 3: the leftmost one giving the $\phi=\pi$ configuration, the rightmost one recognized as the saddle-point configuration from Eq. (18) with $\phi_0=\pi/2$ discussed previously, and the intermediate one giving a spatially nonuniform metastable configuration from Eq. (18). Increasing h beyond $h=1/2$ causes the intersections for the saddle point and nonuniform metastable configurations to move toward each other, until at $h\simeq 0.61$ they coalesce. The activation energy for reversal then vanishes, and reversal takes place spontaneously.

It is generally difficult to derive analytic expressions for the activation energy and field of reversal when $\alpha>\alpha_{\rm crit}$. One exception is the limit $\alpha\to\infty$, where both quantities become independent of the defect strength. When $h=0$, a solution of Eq. (19) is given by $\cos\phi_0=-2/\alpha$ for $\alpha\geqslant 2$. The corresponding configuration from Eq. (18) is shown in Fig. 4(a) and was termed a "solitary dipole" in Ref. 30. The solitary dipole becomes metastable for infinitesimal h, and the saddle-point configuration shown in Fig. 4(b) is given by the pinned soliton-antisoliton pair from Eqs. (12) and (16). Both configurations have $\phi_0=\pi/2$ as $\alpha\to\infty$, so the only important difference between them is given by the dashed curve in Fig. 4(b). Since this dashed curve is exactly half a soliton-antisoliton pair as $h\to 0$ and since $E=\int dx(\partial\phi/\partial x)^2$ on either side of the point-like defect from Eqs. (6) and (11), the energy to nucleate a pinned soliton-antisoliton pair from a metastable solitary dipole becomes $\Delta E_{\rm nuc}=E_{\rm sap}/2$, or in the units of Sec. II,

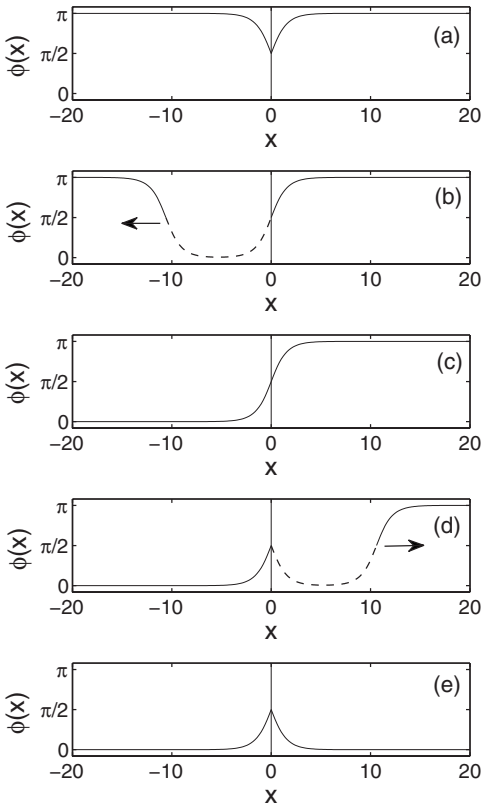

FIG. 4. Reversal mechanism for $\alpha\to\infty$ and infinitesimal h. In (a), a metastable configuration given by a solitary dipole is shown. In (b), a saddle-point configuration given by a pinned soliton-antisoliton pair differs from the solitary dipole by the dashed curve. Following nucleation, the soliton and antisoliton move apart (arrow), leaving a metastable pinned soliton in (c). In (d), a second nucleation event completes reversal, leaving a stable solitary dipole in (e).

$$\Delta E_{\rm nuc}=4\mathcal{A}_r\sqrt{AK}, \tag{25}$$

which corresponds to the energy of one domain wall.[32] Following nucleation, the soliton and antisoliton are driven apart by the applied field, as indicated by the arrow in Fig. 4(b), and a single pinned soliton remains, as shown in Fig. 4(c). This state is also metastable, and nucleation of a second soliton-antisoliton half pair is required before reversal can be completed, as shown in Figs. 4(d) and 4(e). The activation energy for reversal is given by the energy required for a single nucleation event:

$$E_a=\Delta E_{\rm nuc}. \tag{26}$$

Although complete reversal of a 1D ferromagnet requires the nucleation of a soliton and an antisoliton, it is now seen that a point-like defect can break reversal into two steps, each of which requires only half the activation energy for nucleating a soliton-antisoliton pair. Complete reversal will take place at

half the rate of either step in this two-step mechanism.

When $h=1/2$, the pinned soliton-antisoliton pair merges with a configuration given by Eq. (18) with $\phi_0=\pi/2$. In the limit $\alpha\to\infty$, this configuration is a metastable solitary dipole, and the saddle-point and metastable configurations coalesce. The activation energy for reversal then vanishes, and reversal takes place spontaneously. In the units of Sec. II, this field of reversal is given by

$$H_{\rm rev}=\frac{K}{\mu_0 M_s}, \tag{27}$$

which is exactly half the anisotropy field.

IV. RATE PREFACTOR

Analytic evaluation of I_0 is performed in this section for an arbitrary defect strength below the critical value defined in Eq. (20). In this case, a pinned soliton-antisoliton pair is nucleated from a uniform metastable state. A formula for I_0 is derived in Appendix A using Langer's theory[28,29] and is evaluated here analytically in the limit as $h\to 0$. Although it is only assumed that $\alpha<\alpha_{\rm crit}$ in this evaluation, the limit $\alpha\to 0$ will be taken to simplify expressions whenever the dominant behavior remains unaffected. The prefactor I_0 depends on the energy of small deviations, which is considered next.

A. Energy spectrum of small deviations

Small deviations in a planar magnetic configuration of a 1D ferromagnet include both *in-plane* deviations $\delta\phi$ and *out-of-plane* deviations $\delta\theta$. For a soliton-antisoliton pair, these are given by

$$\phi(x)=\phi_{\rm sap}(x)+\delta\phi(x),\quad \theta(x)=\frac{\pi}{2}+\delta\theta(x). \tag{28}$$

Substituting Eq. (28) into Eq. (6), then expanding to second order in $\delta\phi$ and $\delta\theta$, leads to an expression for the energy of small deviations. Assuming an appropriate set of boundary conditions, a basis for the deviations is given by the normalized eigenfunctions $\chi_i^{\varphi,p}$, and deviations can be expressed in terms of the coefficients φ_i and p_j as

$$\delta\phi(x)=\sum_i \varphi_i\chi_i^{\varphi}(x),\quad \delta\theta(x)=\sum_j p_j\chi_j^{p}(x), \tag{29}$$

where the $\chi_i^{\varphi,p}$ satisfy the eigenvalue equations

$$\mathcal{H}^{\varphi}\chi_i^{\varphi}=\lambda_i^{\varphi}\chi_i^{\varphi},\quad \mathcal{H}^{p}\chi_j^{p}=\lambda_j^{p}\chi_j^{p}, \tag{30}$$

and where $\mathcal{H}^{\varphi}$ and $\mathcal{H}^{p}$ are linear differential operators given by

$$\mathcal{H}^{\varphi}=-\frac{d^2}{dx^2}+\frac{1}{\delta_s^2}V_-\left(\frac{x-x_0}{\delta_s},R\right)-\alpha\frac{\partial^2 V_d}{\partial\phi^2}\delta(x) \tag{31}$$

and

$$\mathcal{H}^{p}=-\frac{d^2}{dx^2}+\frac{1}{\delta_s^2}V_+\left(\frac{x-x_0}{\delta_s},R\right)-\alpha\frac{\partial^2 V_d}{\partial\theta^2}\delta(x), \tag{32}$$

with

$$V_{\pm}(\xi,R)=1-2\,\mathrm{sech}^2(\xi+R)-2\,\mathrm{sech}^2(\xi-R)\pm 2\,\mathrm{sech}(\xi+R)\mathrm{sech}(\xi-R), \tag{33}$$

and V_d is given by Eq. (7). In this eigenfunction basis, the energy of small deviations in a pinned soliton-antisoliton pair is given to second order as

$$E_{\rm pin}^{(2)}=E_{\rm pin}+\frac{1}{2}\sum_i \lambda_i^{\varphi}\varphi_i^2+\frac{1}{2}{\sum_j}' \lambda_j^{p}p_j^2, \tag{34}$$

where $E_{\rm pin}$ is the energy of a pinned soliton-antisoliton pair from Eq. (17) and $\lambda_i^{\varphi,p}$ are the eigenvalues from Eq. (30). When $\alpha=0$, the operators $\mathcal{H}^{\varphi}$ and $\mathcal{H}^{p}$ given by Eqs. (31) and (32) correspond to those previously found for in-plane and out-of-plane deviations of an unpinned soliton-antisoliton pair.[4] The terms proportional to α give the contribution due to a single point-like defect.

The energy given by Eq. (2) remains unchanged with respect to uniform rotations of $\boldsymbol{m}$ about the easy axis, leading to a zero eigenvalue in Eq. (34). A uniform rotation of a soliton-antisoliton pair about the easy axis by an infinitesimal angle $d\omega$ results in the out-of-plane deviation $\delta\theta=\sin\phi_{\rm sap}d\omega$: There is no corresponding in-plane deviation to infinitesimal order. In the eigenfunction basis, this implies $\chi_1^p\propto\sin\phi_{\rm sap}$, where

$$\sin\phi_{\rm sap}=\mathrm{sech}(\xi-R)\tanh(\xi+R)-\mathrm{sech}(\xi+R)\tanh(\xi-R), \tag{35}$$

which is an exact solution to the eigenvalue equation in Eq. (30) for out-of-plane deviations with $\lambda_1^p=0$. This zero eigenvalue is denoted by the primed sum in Eq. (34). The eigenfunction given by χ_1^p is nodeless, so λ_1^p is the lowest eigenvalue for out-of-plane deviations.

For the uniform metastable state, in-plane deviations are given by $\phi(x)=\pi+\delta\phi(x)$, while out-of-plane deviations are as in Eq. (28). From Eq. (6), the energy of small deviations in the metastable state to second order becomes

$$E_0^{(2)}=\frac{1}{2}\sum_i \lambda_i^{(0)}\varphi_i^2+\frac{1}{2}\sum_j \lambda_j^{(0)}p_j^2, \tag{36}$$

where the $\lambda_i^{(0)}$ are eigenvalues which solve eigenvalue equations similar to those in Eq. (30) with $\mathcal{H}^{\varphi}=\mathcal{H}^{p}=\mathcal{H}^{(0)}$ and where

$$\mathcal{H}^{(0)}=-\frac{d^2}{dx^2}+\frac{1}{\delta_s^2}-\alpha\delta(x). \tag{37}$$

The eigenvalue equations in Eq. (30) can be treated in a similar way to a 1D Schrödinger equation with a delta-function potential. The soliton and antisoliton in Eq. (12) become unbound ($R\to\infty$) as $h\to 0$, allowing analytic solutions to be constructed for the eigenvalue equations. This is carried out in Appendix B. However, important insight can also be gained using perturbation theory, which is considered next.

B. Half-breathing modes

To understand how the metastable state decays in the presence of a point-like defect, the energy of in-plane devia-

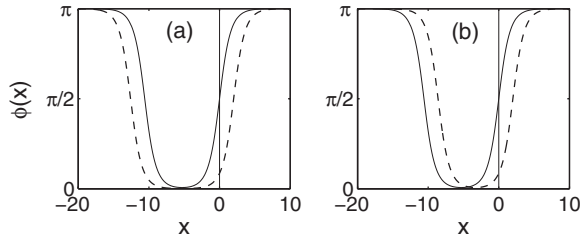

FIG. 5. Deviations (dashed) in a pinned soliton-antisoliton pair (solid) for an infinitesimal defect strength satisfying $\alpha < 2h$. In (a), the breathing mode changes the separation of the soliton and antisoliton. In (b), the translation mode changes the position of the center of mass of the soliton-antisoliton pair.

tions is considered in the limit as $h \to 0$. According to Ref. 33, there are two bound states of the eigenvalue equation with $\mathcal{H}^{\varphi}$ from Eq. (31) when $\alpha=0$ and $R \to \infty$. These are given by $\chi_1^{sap} \propto \mathrm{sech}(\xi+R)+\mathrm{sech}(\xi-R)$ and $\chi_2^{sap} \propto \mathrm{sech}(\xi+R)-\mathrm{sech}(\xi-R)$, with eigenvalues

$$\lambda_1^{sap} \simeq -8e^{-2R}, \tag{38}$$

$$\lambda_2^{sap} = 0. \tag{39}$$

The corresponding deviations in a pinned soliton-antisoliton pair are shown in Fig. 5. In Fig. 5(a), it is seen that $\chi_1^{sap} \propto d\phi_{\mathrm{sap}}/dR$ gives an infinitesimal change in the separation of the soliton and antisoliton (called a *breathing mode*), while in Fig. 5(b), $\chi_2^{sap} \propto d\phi_{\mathrm{sap}}/dx$ gives an infinitesimal change in the position of the center of mass of a soliton-antisoliton pair (called a *translation mode*). The zero eigenvalue in Eq. (39) implies a soliton-antisoliton pair has translational symmetry in a ferromagnet with no defects.

Simple insight into the modifications due to a point-like defect can be found using first-order perturbation theory for an infinitesimal defect strength. Assuming that the unperturbed eigenfunctions are given by the bound states χ_1^{sap} and χ_2^{sap}, the perturbed bound-state eigenvalues are eigenvalues of the 2×2 matrix:

$$\langle \chi_i^{sap} | \mathcal{H}^{\varphi} | \chi_j^{sap} \rangle = \delta_{ij}\lambda_j^{sap} - \alpha \chi_i^{sap} \left. \frac{\partial^2 V_d}{\partial \phi^2} \chi_j^{sap} \right|_{x=0}, \tag{40}$$

where $i,j=1,2$. The matrix elements can be found by normalizing χ_1^{sap} and χ_2^{sap} and using $\xi=(x-x_0)/\delta_s$ with Eqs. (13) and (16) as $R \to \infty$, along with Eq. (7) and $\phi_{\mathrm{sap}}=\pi/2$ at $x=0$. The eigenvalues of this matrix are

$$\lambda^{\pm} = \frac{\alpha + 2\delta_s \lambda_1^{sap} \pm \sqrt{\alpha^2 + (2\delta_s \lambda_1^{sap})^2}}{4\delta_s}. \tag{41}$$

When $|\alpha| \ll |2\delta_s \lambda_1^{sap}|$, the eigenvalues become $\lambda^+ = \lambda_1^{sap}$ and $\lambda^- = \alpha/4\delta_s$. The correction due to a point-like defect is given by λ^- and implies that the energy to change the position of the center of mass of a pinned soliton-antisoliton pair becomes proportional to the defect strength—that is, a point-like defect breaks translational symmetry. When

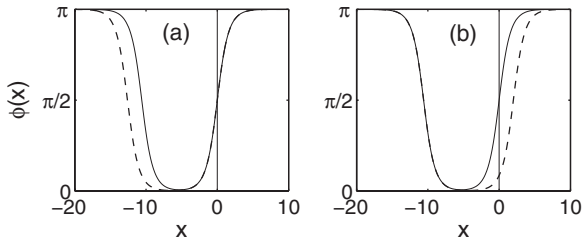

FIG. 6. Deviations (dashed) in a pinned soliton-antisoliton pair (solid) for an infinitesimal defect strength satisfying $\alpha > 2h$. In (a), one half-breathing mode changes the separation of the soliton and antisoliton without unpinning the soliton from the point-like defect at $x=0$. In (b), the other half-breathing mode does unpin this soliton.

$|\alpha| \gg |2\delta_s \lambda_1^{sap}|$, the eigenvalues become $\lambda^- = \lambda_1^{sap}/2$ and $\lambda^+ = \alpha/2\delta_s$, while the deviations are linear combinations of χ_1^{sap} and χ_2^{sap}, as shown in Fig. 6. These deviations are called *half-breathing modes*, as the change in the separation of a soliton and antisoliton is now due only to one member of the soliton-antisoliton pair, instead of both. Half-breathing modes decouple the mechanism for unpinning a soliton-antisoliton pair from a point-like defect, from the mechanism for expansion and contraction of the nucleus of critical size, allowing magnetization reversal to proceed even when the applied field is too weak to completely unpin a soliton-antisoliton pair. In fact, retaining λ_1^{sap} to lowest order in Eq. (41), the eigenvalue for the half-breathing mode in Fig. 6(b) is given by $\lambda^+ = \alpha/2\delta_s + \lambda_1^{sap}/2$. After making use of Eqs. (13) and (38) as $h \to 0$, this can also be written as $\lambda^+ = \alpha/2 - h$. This eigenvalue will no longer be negative when $h < \alpha/2$, meaning that one member of the soliton-antisoliton pair will then remain pinned to the point-like defect.

When the defect strength is not infinitesimal, there is a correction to the half-breathing mode in the vicinity of the defect. The corrected half-breathing mode has been found in Appendix B and is shown in Fig. 7. Comparison of Figs. 6(b) and 7(a) shows that the pinned soliton becomes strongly localized to the pinning site using the corrected eigenfunction. The corrected eigenvalue from Eq. (B16) is plotted in Fig. 7(b) and is seen to join the bottom of the scattering-state spectrum as $\alpha \to \infty$. However, when $\alpha < \alpha_{\mathrm{crit}}$, it is clear from this figure that λ_2^{φ} is well approximated by its $\alpha \to 0$ value. Therefore, assuming $\alpha > 2h$ as $h \to 0$, the half-breathing mode eigenvalues can be approximated as

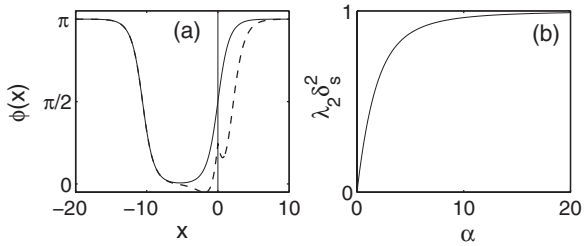

FIG. 7. Half-breathing mode in the vicinity of a point-like defect for arbitrary defect strength. In (a), the deviation (dashed) in a pinned soliton-antisoliton pair (solid) from the corrected eigenfunction is shown. In (b), the corrected eigenvalue as a function of α is shown.

$$\lambda_1^{\varphi} \simeq -4e^{-2R}, \tag{42}$$

$$\lambda_2^{\varphi} \simeq \frac{\alpha}{2\delta_s}. \tag{43}$$

C. Prefactor evaluation

Applying Langer's theory to a dilute gas of pinned soliton-antisoliton pairs at nonzero applied field leads to a formula for I_0 which is derived in Appendix A. This formula depends on the energy eigenvalues discussed in the previous sections and is given by

$$I_0 = \frac{\kappa}{\pi} N_d \mathcal{R} \sqrt{\frac{\beta}{2\pi}} \sqrt{\frac{\Pi_i \lambda_i^{(0)}}{|\lambda_1^{\varphi}| \Pi_j{}' \lambda_j^{\varphi}}} \sqrt{\frac{\Pi_i \lambda_i^{(0)}}{\Pi_j{}' \lambda_j^{p}}}, \tag{44}$$

where κ is the growth rate of the linearly unstable deviation in a pinned soliton-antisoliton pair and is the only term in I_0 due to dynamics, N_d is the number of point-like defects (the defects are assumed to be identical and spaced widely apart), and $\mathcal{R}=4\pi$ is the zero-eigenvalue contribution from the continuous symmetry of a pinned soliton-antisoliton pair with respect to rotations about the easy axis and follows from Eqs. (35) and (A7) as $R \to \infty$. The single negative eigenvalue from Eq. (42) contributes through the modulus $|\lambda_1^{\varphi}|$. All other eigenvalues are positive and can be combined into a single term which describes the difference in entropy between the activated and metastable states,[1] called the *activation entropy*. The entropy and dynamics terms are now evaluated.

1. Entropy term

As $h \to 0$, only the lowest energy deviations in a pinned soliton-antisoliton pair will be significantly affected by the applied field. The lowest order h dependence is therefore retained in the bound-state eigenvalues of Eq. (30), while the scattering-state eigenvalues are approximated by their value at $h=0$. Each ratio of positive eigenvalues in Eq. (44) then becomes

$$\lim_{h \to 0} \frac{\Pi_i \lambda_i^{(0)}}{\Pi_j{}' \lambda_j^{\varphi,p}} = \frac{\lambda_1^{(0)} \Pi_k \lambda_k^{(0)}}{\lambda_2^{\varphi,p} \Pi_{k'} \lambda_{k'}^{\varphi,p}}, \tag{45}$$

where λ_2^{φ} is given by Eq. (43), $\lambda_2^{p} \simeq 8\exp(-2R)$ from Refs. 33 and 34 (it is shown in Appendix B that out-of-plane deviations in a soliton-antisoliton pair are unaffected by a point-like defect), $\lambda_1^{(0)} = \delta_s^{-2} - (\alpha/2)^2$ from Appendix B, and $\lambda_k^{(0)}$ and $\lambda_{k'}^{\varphi,p}$ are the scattering-state eigenvalues of Eq. (30) at $h=0$ and are also found in Appendix B.

The number of bound states for deviations in a soliton-antisoliton pair actually depends on h, since nonzero h in Eq. (10) leads to the time-independent double sine-Gordon equation, which has been shown to contain an additional bound state called an "internal" mode.[35] However, the method used here for evaluating products of scattering-state eigenvalues has been shown to give the correct result in the limit $h \to 0$ when defects are not included.[4] Next, it will be demonstrated that inclusion of a point-like defect creates no new bound states for deviations in a pinned soliton-antisoliton pair, so this argument remains unchanged.

The scattering-state eigenvalues can be determined by applying boundary conditions to the eigenfunctions from Appendix B. The scattering-state eigenfunctions for deviations in the $\phi=\pi$ state can be written in terms of even-parity (e) and odd-parity (o) states as

$$\chi_k^{(e)}(x \to +\infty) \propto \cos[kx + \Delta(k)], \tag{46}$$

$$\chi_k^{(e)}(x \to -\infty) \propto \cos kx, \tag{47}$$

$$\chi_k^{(o)}(x \to \pm\infty) \propto \sin kx, \tag{48}$$

where the phase shift $\Delta(k)$ is due to the point-like defect and is given by

$$\Delta(k) = \arctan\left(\frac{\alpha}{k}\right). \tag{49}$$

Applying periodic boundary conditions $\chi_k(-L/2) = \chi_k(L/2)$ and $\chi_k'(-L/2) = \chi_k'(L/2)$, the k values of odd-parity states are given by

$$k = \frac{2\pi n}{L}, \tag{50}$$

while the k values of even-parity states are determined from solving

$$k = \frac{2\pi n}{L} - \frac{\Delta(k)}{L}. \tag{51}$$

When $\alpha=0$, then $\Delta(k)=0$, and the lowest k value corresponds to $n=1$ for odd-parity states and $n=0$ for even-parity states. When $\alpha \neq 0$, the following argument from Ref. 36 can be used. As $L \to \infty$, k with any finite n tends to zero and $\Delta(k \to 0) = \pi/2$ for the lowest k values. According to Eq. (51), the lowest even-parity state must now be $n=1$, as $n=0$ would give $k<0$. The phase shift due to the defect therefore results in one less even-parity state: The lowest energy scattering state is trapped by the defect and becomes the bound state found in Appendix B.

The density of scattering states follows from Eqs. (50) and (51) in the limit $L \to \infty$. Using $\rho(k) = dn/dk$ for both even and odd-parity states, and including an additional delta-function contribution at $k=0$, yields

$$\rho(k) = \frac{L}{\pi} + \frac{1}{2\pi}\frac{d\Delta(k)}{dk} - \frac{3}{4}\delta(k). \tag{52}$$

The delta-function contribution ensures that the total number of states for $\alpha=0$ equals the total number of bound and scattering states when $\alpha \neq 0$ (where $N_b=1$ from the previous discussion):

$$\int_0^{\infty} dk \left[\frac{L}{\pi} - \rho(k)\right] = N_b. \tag{53}$$

The scattering-state eigenfunctions for in-plane deviations in a pinned soliton-antisoliton pair can also be written in terms of even-parity and odd-parity states. Including the contribution made by the soliton infinitely far from the defect then yields

$$\chi_k^{\varphi(e)}(x \to +\infty) \propto \cos[kx + \Delta^{sap}(k) - \Delta^{\alpha}(k)], \tag{54}$$

$$\chi_k^{\varphi(e)}(x \to -\infty) \propto \cos[kx - \Delta^{sap}(k)], \tag{55}$$

$$\chi_k^{\varphi(o)}(x \to \pm\infty) \propto \sin[kx \pm \Delta^{sap}(k)], \tag{56}$$

where the phase shift is now due to both the soliton-antisoliton pair,

$$\Delta^{sap}(k) = 2\arctan\left(\frac{1}{k\delta}\right), \tag{57}$$

and the point-like defect,

$$\Delta^{\alpha}(k) = \arctan\left[\frac{\alpha k \delta^2}{2(1+k^2\delta^2)}\right]. \tag{58}$$

Applying periodic boundary conditions, the k values of the odd-parity states are determined from

$$k = \frac{2\pi n}{L} - \frac{2\Delta^{sap}(k)}{L}, \tag{59}$$

while the k values of the even-parity states are determined from

$$k = \frac{2\pi n}{L} - \frac{2\Delta^{sap}(k)}{L} + \frac{\Delta^{\alpha}(k)}{L}. \tag{60}$$

Since $\Delta^{\alpha}(k \to 0) = 0$ and $\Delta^{sap}(k \to 0) = \pi$, the lowest k value corresponds to $n=2$ for the odd-parity states and $n=1$ for the even-parity states. This means that there are two fewer scattering states than in the $\Delta^{sap}(k)=0$ case (where the lowest k values correspond to $n=1$ and $n=0$, respectively). The two lowest energy scattering states are trapped by the soliton-antisoliton pair to become the two half-breathing modes λ_1^{φ} and λ_2^{φ} from Eqs. (42) and (43). The defect does not trap any scattering states in this case. The density of scattering states following from Eqs. (59) and (60) in the limit $L \to \infty$ is given by

$$\rho^{\varphi}(k) = \frac{L}{\pi} + \frac{2}{\pi}\frac{d\Delta^{sap}(k)}{dk} - \frac{1}{2\pi}\frac{d\Delta^{\alpha}(k)}{dk}. \tag{61}$$

Similarly, the density of scattering states for out-of-plane deviations is found to be

$$\rho^{p}(k) = \frac{L}{\pi} + \frac{2}{\pi}\frac{d\Delta^{sap}(k)}{dk}, \tag{62}$$

as out-of-plane deviations in a soliton-antisoliton pair are unaffected by a point-like defect.

It is now possible to evaluate the ratios of scattering-state eigenvalues using

$$\frac{\Pi_k \lambda_k^{(0)}}{\Pi_{k'} \lambda_{k'}^{i}} = \exp\left\{\int_0^{\infty} dk[\rho(k) - \rho^{i}(k)]\ln(\delta_s^{-2} + k^2)\right\}, \tag{63}$$

where $i = \varphi, p$ and $\rho(k)$, $\rho^{\varphi}(k)$, and $\rho^{p}(k)$ are given by Eqs. (52), (61), and (62). The integrals in Eq. (63) have been evaluated in Appendix C, and the ratios of scattering-state eigenvalues are found to be

$$\frac{\Pi_k \lambda_k^{(0)}}{\Pi_{k'} \lambda_{k'}^{p}} = \frac{16\delta_s^{-5/2}}{\sqrt{\delta_s^{-1} + \alpha}} \tag{64}$$

and

$$\frac{\Pi_k \lambda_k^{(0)}}{\Pi_{k'} \lambda_{k'}^{\varphi}} = \frac{16\delta_s^{-5/2}(\delta_s^{-1} + \delta_s^{-1}A^{-})^{\alpha\delta_s[1+(A^{-})^2]/\{4A^{-}[(A^{+})^2-(A^{-})^2]\}}}{\sqrt{\delta_s^{-1} + \alpha}(\delta_s^{-1} + \delta_s^{-1}A^{+})^{\alpha\delta_s[1+(A^{+})^2]/\{4A^{+}[(A^{+})^2-(A^{-})^2]\}}}, \tag{65}$$

where

$$A^{\pm} = \sqrt{1 + \frac{\alpha^2\delta_s^2}{8} \pm \sqrt{\frac{\alpha^2\delta_s^2}{4} + \frac{\alpha^4\delta_s^4}{64}}}. \tag{66}$$

Using these expressions in Eq. (45) yields the activation entropy given by the ratios of positive eigenvalues. When $\alpha < \alpha_{\text{crit}}$, the activation entropy is dominated by the $\alpha \to 0$ contribution from in-plane deviations:

$$\lim_{h \to 0} \frac{\Pi_i \lambda_i^{(0)}}{\Pi_j{}' \lambda_j^{\varphi}} \simeq \frac{32\delta_s^{-3}}{\alpha}, \tag{67}$$

so the activation entropy *decreases* as α increases. The α dependence in Eq. (67) is directly due to the energy eigenvalue λ_2^{φ}: A point-like defect breaks translational symmetry, and the energy to unpin a soliton-antisoliton pair from a point-like defect is proportional to the defect strength. Increasing α localizes a pinned soliton-antisoliton pair more strongly to a defect site, confining nucleation to a smaller and smaller volume of space and therefore decreasing the associated activation entropy.

2. Dynamics term

The dissipative magnetization dynamics obeys the Landau-Lifshitz equation given by Eq. (4). In spherical-polar coordinates and the characteristic length, energy, and time scales defined in Eq. (5), the Landau-Lifshitz equation becomes

$$\frac{\partial\theta}{\partial t} = -\Lambda\frac{\delta E}{\delta\theta} - \frac{1}{\sin\theta}\frac{\delta E}{\delta\phi},$$

$$\sin\theta\frac{\partial\phi}{\partial t} = \frac{\delta E}{\delta\theta} - \frac{\Lambda}{\sin\theta}\frac{\delta E}{\delta\phi}. \tag{68}$$

Linearizing Eq. (68) about a soliton-antisoliton pair, and assuming that E is given by Eq. (34), leads to a pair of coupled linear differential equations for $p_i(t)$ and $\varphi_j(t)$:

$$\dot{p}_i = -\Lambda\lambda_i^{p} p_i - \lambda_j^{\varphi}\varphi_j,$$

$$\dot{\varphi}_j = \lambda_i^{p} p_i - \Lambda\lambda_j^{\varphi}\varphi_j. \tag{69}$$

When an out-of-plane deviation is given by the rotation mode p_1, the λ_i^{p} in Eq. (69) vanish, and the linearized equations decouple. Assuming that the linearly unstable deviation is given by the rotation mode for out-of-plane deviations and the half-breathing mode for in-plane deviations, $[p_i(t), \varphi_j(t)] \propto (p_1, \varphi_1)\exp(\lambda^{+}t)$, where $\kappa = \lambda^{+}\tau^{-1}$, and inserting this into Eq. (69), yields

$$\kappa = \Lambda |\lambda_1^{\varphi}| \tau^{-1}. \tag{70}$$

Since the half-breathing mode eigenvalue λ_1^{φ} is $\lambda_1^{\varphi} = \lambda_1^{sap}/2$, the soliton and antisoliton move apart at half the rate of an unpinned soliton-antisoliton pair in an applied field, decreasing κ by a half. The growth rate also depends on $\Lambda\tau^{-1}$, which is the rate of energy dissipation due to Landau-Lifshitz dynamics.

3. Total prefactor

When $\alpha < \alpha_{\text{crit}}$, the dominant behavior in I_0 remains unchanged in the $\alpha \to 0$ limit. Combining the previous results into Eq. (44), and taking the $\alpha \to 0$ limit, yields

$$I_0 = 32 \frac{\Lambda}{\tau} N_d \sqrt{\frac{2\beta}{\pi\alpha}}. \tag{71}$$

This expression increases with the number of point-like defects N_d but decreases with increase in the defect strength α. The reason for the α dependence is the same as that given previously: Broken translational symmetry means that the activation entropy for nucleating a pinned soliton-antisoliton pair decreases as the soliton-antisoliton pair becomes more strongly localized to a pinning site. Conversely, decreasing α results in a pinned soliton-antisoliton pair becoming less and less localized, eventually restoring translational symmetry when α goes to zero. In this case, the emerging zero-energy eigenvalue must be treated by integrating over the translation mode.[28,29] Increasing N_d increases the number of possible nucleation sites, thereby increasing I_0. The temperature dependence β appears due to rotational symmetry about the easy axis, and $\Lambda\tau^{-1}$ is the rate at which energy is dissipated through damped soliton motion during magnetization reversal.

V. SUMMARY AND DISCUSSION

This work has demonstrated that point-like defects in the magnetic anisotropy can facilitate nucleation of soliton-antisoliton pairs and therefore enhance the rate of thermally activated magnetization reversal. It was shown that a spatially nonuniform metastable state is created when the defect strength lies above a critical value, leading to a significant reduction in the activation energy and field of reversal. The reversal-rate prefactor was also found to be modified by point-like defects, primarily due to broken translational symmetry and the localization of nucleation to the defect sites.

In Sec. III, it was found that the spatially uniform metastable state becomes unstable and the new metastable state is spatially nonuniform when the applied field and defect strength exceed certain critical values. As the applied field tends to zero, the lowest activation energy for a soliton-antisoliton pair pinned to a point-like defect was found to be exactly half that of an unpinned pair when the defect strength becomes large. The smallest field of reversal was found to be exactly half of the anisotropy field.

In Sec. IV, through exact determination of the reversal-rate prefactor for point-like defects below the critical defect strength, the reversal-rate prefactor was found to increase with the number of point-like defects and to decrease with increase in the defect strength. An increase in the number of point-like defects creates more possible nucleation sites for pinned soliton-antisoliton pairs, while an increase in the defect strength decreases the activation entropy associated with nucleation as the pinned soliton-antisoliton pairs become more strongly localized to the defect sites. It was shown that half-breathing modes allow magnetization reversal to proceed when the applied field is too weak to completely unpin a soliton-antisoliton pair from a point-like defect.

More generally, the total rate of magnetization reversal for a 1D uniaxial ferromagnet with point-like defects is the sum of rates for the nucleation of soliton-antisoliton pairs which are unpinned,[4] pinned at point-like defects (as investigated here), and pinned at the sample ends.[5] In particular, a crossover from heterogeneous to homogeneous nucleation is expected to take place above a critical sample length for nucleation at the sample ends and below a critical density of defects for nucleation at point-like defects, as found in Ref. 31. At zero applied field, the activation energy for nucleation at the sample ends is exactly half that for a soliton-antisoliton pair.[5] This is also the minimum activation energy for nucleation at a point-like defect at zero applied field; however, when the applied field is nonzero, the field of reversal is always lower for nucleation at a point-like defect. Nucleation at a point-like defect can therefore be the dominant mechanism for magnetization reversal when either the defect strength is large or when many defects are present.

ACKNOWLEDGMENTS

The author would like to thank R. L. Stamps and I. McArthur for informative discussions.

APPENDIX A: NUCLEATION RATE OF PINNED SOLITON-ANTISOLITON PAIRS

The nucleation rate of pinned soliton-antisoliton pairs from a uniform metastable state follows from the application of Langer's theory.[28,29] This involves computing the free energy density F of a stable state—in this case, a dilute gas of pinned soliton-antisoliton pairs at zero applied field—then finding the analytic continuation of F, denoted by $\tilde{F}$, when the applied field is nonzero, and the uniform state becomes metastable. The rate of nucleation I is then related to the imaginary part of $\tilde{F}$ as

$$I = \frac{\kappa}{\pi} L\beta \,\mathrm{Im}\,\tilde{F}, \tag{A1}$$

where L is the system length, $\beta = 1/k_B T$, and κ is the growth rate of the linearly unstable deviation in a pinned soliton-antisoliton pair.[28,29]

Ideal gas phenomenology can be applied to a soliton gas when the equilibrium density of solitons is small, and interactions become negligible.[37–39] The free energy density F is then given by that for an ideal gas (see Ref. 40, for example):

$$F = -\frac{n_s}{\beta}, \tag{A2}$$

where n_s is the equilibrium density of solitons, given by $n_s = Q_1/L$, and Q_1 is the single-soliton partition function; the chemical potential has been set to zero as n_s depends only on the temperature.[37–39] In the present case, a single soliton corresponds to a pinned soliton-antisoliton pair, and n_s becomes small whenever $\beta E_{\text{pin}} \gg 1$ holds. The form of Eq. (A2) does not depend on the number of available pinning sites, as $\exp(Q_1) \simeq 1 + Q_1$ in the small density limit; so, the main contribution to the grand partition function is due to a single pinned soliton-antisoliton pair. However, the number of available pinning sites does enter into the expression for Q_1, as will be seen.

The single-soliton partition function Q_1 is related to Δf—the Helmholtz free energy of adding a single soliton to the system—as

$$Q_1 \equiv e^{-\beta \Delta f} = \frac{\mathcal{Z}_s}{\mathcal{Z}_0}, \tag{A3}$$

where $\mathcal{Z}_0$ is the partition function before adding the soliton (calculated for $\phi = \pi$) and $\mathcal{Z}_s$ is the partition function after adding the soliton (calculated for a single pinned soliton-antisoliton pair). The partition functions $\mathcal{Z}_0$ and $\mathcal{Z}_s$ can be calculated using a path integral approach (cf. Ref. 39):

$$\mathcal{Z} = \int D\phi(x) \int D\theta(x) e^{-\beta E[\phi(x), \theta(x)]}. \tag{A4}$$

Using the energy expression from Eq. (36), $\mathcal{Z}_0$ is then approximated as a product of Gaussian integrals, one for each in-plane and out-of-plane deviation, yielding

$$\mathcal{Z}_0 = \mathcal{N} \prod_i [\lambda_i^{(0)}]^{-1/2} \prod_j [\lambda_j^{(0)}]^{-1/2}, \tag{A5}$$

where $\mathcal{N}$ is a product of $\sqrt{2\pi/\beta}$ factors, one from each integral. In a uniform system of length L, a soliton-antisoliton pair is equally likely to be found at any location, and $\mathcal{Z}_s \propto L$. For a system with N_d widely spaced identical defects, $\mathcal{Z}_s$ for a pinned soliton-antisoliton pair becomes $\mathcal{Z}_s \propto 2N_d$—a choice of pinning either the soliton or the antisoliton leads to a factor of 2. Using the energy expression from Eq. (34), $\mathcal{Z}_s$ is then

$$\mathcal{Z}_s = e^{-\beta E_{\text{pin}}} \mathcal{N} \prod_i {}' [\lambda_i^{\varphi}]^{-1/2} \prod_j {}' [\lambda_j^{p}]^{-1/2} 2N_d \frac{1}{\sqrt{\pi}} \times \int d\varphi_1 e^{-\lambda_1^{\varphi} \varphi_1^2} \sqrt{\frac{\beta}{2\pi}} \int dp_1, \tag{A6}$$

where the factor $\mathcal{N}$ is the same as in Eq. (A5), and the integrals over φ_1 and p_1 have not been performed because they are potentially divergent.

The integral over p_1 is potentially divergent due to the vanishing of λ_1^p from rotational symmetry. A uniform rotation of a soliton-antisoliton pair about the easy axis by an infinitesimal angle $d\omega$ results in the out-of-plane deviation $\delta\theta = \sin \phi_{\text{sap}} d\omega$. The same out-of-plane deviation results from an infinitesimal change in the appropriate eigenfunction coefficient: $\delta\theta = \chi_1^p dp_1$. Using these relations to perform a change of variable from dp_1 to $d\omega$, then integrating over the range of values available to $d\omega$, yields

$$\int dp_1 = |\sin \phi_{\text{sap}}| \int_0^{2\pi} d\omega,$$

$$= 2\pi \sqrt{\int_{-L/2}^{L/2} dx \sin^2 \phi_{\text{sap}}},$$

$$\equiv \mathcal{R}, \tag{A7}$$

where the Jacobian of transformation is given by $|\sin \phi_{\text{sap}}|$, since $|\chi_1^p| = 1$ due to normalization.

At zero applied field, λ_1^{φ} also vanishes, and the integral over φ_1 can be treated analogously to that for p_1—except the continuous symmetry now involves translations instead of rotations. For the integral to converge when the applied field is nonzero, the path of integration must be distorted into the complex plane.[28,41,42] Carrying this out yields $\tilde{\mathcal{Z}}_s$, the analytic continuation of $\mathcal{Z}_s$, as

$$\tilde{\mathcal{Z}}_s = e^{-\beta E_{\text{pin}}} \mathcal{N} \prod_i {}' [\lambda_i^{\varphi}]^{-1/2} \prod_j {}' [\lambda_j^{p}]^{-1/2} 2N_d \frac{1}{\sqrt{\pi}} \times \int_0^{\pm i\infty} d\varphi_1 e^{|\lambda_1^{\varphi}| \varphi_1^2} \mathcal{R} \sqrt{\frac{\beta}{2\pi}}, \tag{A8}$$

where the original path of integration for φ_1 has been distorted along the imaginary axis to ensure that the integral is convergent, and only the half interval is integrated over; the other half interval corresponds to values of φ_1 which have effectively been included in the Gaussian approximation for $\mathcal{Z}_0$—this cancels a factor of 2 in the final result. Combining results, and substituting into Eq. (A1), yields

$$I = \frac{\kappa}{\pi} N_d \mathcal{R} \sqrt{\frac{\beta}{2\pi}} \sqrt{\frac{\Pi_i \lambda_i^{(0)}}{|\lambda_1^{\varphi}| \Pi_j {}' \lambda_j^{\varphi}}} \sqrt{\frac{\Pi_i \lambda_i^{(0)}}{\Pi_j {}' \lambda_j^{p}}} e^{-\beta E_{\text{pin}}}. \tag{A9}$$

APPENDIX B: SCHRÖDINGER STATES AT ZERO FIELD

The Schrödinger-type eigenvalue equations given by Eqs. (30)–(33) are solvable analytically when $h = 0$. In this case, the soliton and antisoliton in Eq. (12) become unbound ($R \to \infty$), and the interaction term in Eq. (33) vanishes. Deviations in a soliton pinned to a point-like defect are first treated, followed by deviations in $\phi = \pi$.

1. Pinned soliton states

At zero field, the eigenvalue equations from Eqs. (30)–(33) for in-plane and out-of-plane deviations in a pinned soliton-antisoliton pair become

$$-\frac{d^2 \chi_i^{\varphi}}{dx^2} + \left[\frac{1}{\delta_s^2} V\left(\frac{x - x_0}{\delta_s}, R \right) + \alpha \delta(x) \right] \chi_i^{\varphi} = \lambda_i^{\varphi} \chi_i^{\varphi} \tag{B1}$$

and

$$-\frac{d^2\chi_i^p}{dx^2}+\frac{1}{\delta_s^2}V\left(\frac{x-x_0}{\delta_s},R\right)\chi_i^p=\lambda_i^p\chi_i^p, \tag{B2}$$

where

$$V(\xi,R)=1-2\,\mathrm{sech}^2(\xi+R)-2\,\mathrm{sech}^2(\xi-R). \tag{B3}$$

When $\alpha=0$, the "potential" of these Schrödinger-type equations is given by two independent wells of the form $-2\delta_s^{-2}\,\mathrm{sech}^2(\xi\pm R)$. Making use of Ref. 43, the eigenfunctions consist of two bound states:

$$\chi_{1,2}^{\varphi,p}\propto\mathrm{sech}\left(\frac{x-x_0}{\delta_s}\pm R\right), \tag{B4}$$

with eigenvalue $\lambda_{1,2}^{\varphi,p}=0$, and a continuum of scattering states,

$$\chi_k^{\varphi,p}\propto\left[-ik\delta_s+\tanh\left(\frac{x-x_0}{\delta_s}\pm R\right)\right]e^{ikx}, \tag{B5}$$

with eigenvalue $\lambda_k^{\varphi,p}=\delta_s^{-2}+k^2$. The single $\exp(ikx)$ term in Eq. (B5) implies that there is no reflection from the well potentials, and all waves are transmitted.

When $\alpha\neq 0$, the potential of Eq. (B1) includes a delta function, and waves are reflected. Integrating Eq. (B1) from $-\varepsilon$ to ε, and letting $\varepsilon\to 0$, yields the consistency condition

$$\left.\frac{d\chi_i^\varphi}{dx}\right|_{x=0^+}-\left.\frac{d\chi_i^\varphi}{dx}\right|_{x=0^-}=\alpha\chi_i^\varphi(0). \tag{B6}$$

The scattering-state eigenfunctions of Eq. (B1) can be constructed in an analogous manner to the scattering of plane waves from a well potential in 1D quantum mechanics. Carrying this out for the soliton (or antisoliton) in the vicinity of the point-like defect at $x=0$ yields

$$\chi_k^\varphi=\begin{cases}Af(x)e^{ikx}+Bf^*(x)e^{-ikx}, & x>0\\ Cf(x)e^{ikx}, & x<0,\end{cases} \tag{B7}$$

where $f(x)=-ik\delta_s+\tanh(x/\delta_s)$ is due to the term in brackets in Eq. (B5) after making use of Eqs. (13) and (16) as $R\to\infty$, and $f^*(x)$ denotes the complex conjugate of $f(x)$. Choosing the constants B and C so that $\chi_k^\varphi(0^-)=\chi_k^\varphi(0^+)$ and Eq. (B6) are both satisfied leads to

$$\frac{B}{A}=\frac{-i\alpha k\delta_s^2}{2(1+k^2\delta_s^2)-i\alpha k\delta_s^2} \tag{B8}$$

and

$$\frac{C}{A}=\frac{2(1+k^2\delta_s^2)}{2(1+k^2\delta_s^2)-i\alpha k\delta_s^2}. \tag{B9}$$

The antisoliton (or soliton) which is infinitely far from the defect has $B=0$ and $C=A$. The constant A is determined from the normalization of χ_k^φ. Upon choosing

$$A=\frac{1}{\sqrt{2\pi(1+k^2\delta^2)}}, \tag{B10}$$

and taking the $L\to\infty$ limit, the orthogonality condition for the scattering-state eigenfunctions given by Eq. (B7) becomes

$$\int_{-\infty}^{\infty}dx\chi_k^{\varphi*}(x)\chi_{k'}^\varphi(x)=\delta(k-k')+\frac{B}{A}\delta(k+k'), \tag{B11}$$

where B/A is from Eq. (B8). The bound state in the vicinity of the defect (denoted χ_2^φ) given by Eq. (B4) is no longer orthogonal to these scattering states, since

$$\int_{-\infty}^{\infty}dx\chi_k^\varphi(x)\mathrm{sech}\left(\frac{x}{\delta_s}\right)=2\delta_sB, \tag{B12}$$

which does not vanish for nonzero α. However, a new bound state which is orthogonal to χ_k^φ can be constructed to $O(\alpha)$ by making use of Eq. (B11), yielding

$$\chi_2^\varphi=\frac{1}{\sqrt{N}}\left[\mathrm{sech}\left(\frac{x}{\delta_s}\right)-2\delta_s\int_{-\infty}^{\infty}dkB^*\chi_k^\varphi(x)\right], \tag{B13}$$

where χ_k^φ are the eigenfunctions from Eq. (B7), $N=2\delta_s-4\delta_s^2\int_{-\infty}^{\infty}dk|B|^2$ ensures normalization, and B^* is the complex conjugate of B. The bound-state eigenvalue is then found to $O(\alpha^2)$ by inserting Eq. (B13) into

$$\lambda_2^\varphi=\int_{-\infty}^{\infty}dx\chi_2^{\varphi*}\mathcal{H}^\varphi\chi_2^\varphi, \tag{B14}$$

with $\mathcal{H}^\varphi=-d^2/dx^2+\delta_s^{-2}[1-2\,\mathrm{sech}^2(x/\delta_s)]+\alpha\delta(x)$. Making use of $\mathcal{H}^\varphi\chi_k^\varphi=(\delta_s^{-2}+k^2)\chi_k^\varphi$ for the scattering-state eigenfunctions in Eq. (B7) and the fact that $\mathcal{H}^\varphi$ is Hermitian yields

$$\lambda_2^\varphi=\frac{1}{N}\left[\alpha-4\delta_s^2\int_{-\infty}^{\infty}dk(\delta_s^{-2}+k^2)|B|^2\right]. \tag{B15}$$

The integral in Eq. (B15) and normalization factor N can be calculated using the method of contour integration. The results give

$$\lambda_2^\varphi=\frac{\alpha(1-\alpha\delta_sI_1)}{\delta_s(2-\alpha^2\delta_s^2I_2)}, \tag{B16}$$

where

$$I_1=\frac{1}{2(A^++A^-)}, \tag{B17}$$

$$I_2=\frac{(A^++A^-)(A^--A^+)+A^+(1+A^-)(1-A^-)-A^-(1+A^+)(1-A^+)}{2(1+A^+)(1-A^+)(1+A^-)(1-A^-)(A^++A^-)(A^+-A^-)}, \tag{B18}$$

and

$$A^{\pm} = \sqrt{1 + \frac{\alpha^2\delta_s^2}{8} \pm \sqrt{\frac{\alpha^2\delta_s^2}{4} + \frac{\alpha^4\delta_s^4}{64}}}. \tag{B19}$$

The eigenfunction from Eq. (B13) can also be found using the method of contour integration. The result is

$$\chi_2^{\varphi} \propto \operatorname{sech}\left(\frac{x}{\delta_s}\right) + \frac{\alpha\delta_s}{4}\left[\frac{x}{\delta_s}\tanh\left(\frac{x}{\delta_s}\right) + \frac{|x|}{\delta_s} - 1\right]e^{-|x|/\delta_s}. \tag{B20}$$

2. Uniform defect states

The eigenvalue equations for deviations in $\phi=\pi$ are similar to those in Eq. (30), but with $\mathcal{H}^{\varphi}$ and $\mathcal{H}^{p}$ given by Eq. (37). This yields

$$-\frac{d^2\chi_i}{dx^2} + \left[\frac{1}{\delta_s^2} - \alpha\delta(x)\right]\chi_i = \lambda_i^{(0)}\chi_i. \tag{B21}$$

Integrating Eq. (B21) from $-\varepsilon$ to ε, and letting $\varepsilon \to 0$, yields the consistency condition

$$\left.\frac{d\chi_i}{dx}\right|_{x=0^+} - \left.\frac{d\chi_i}{dx}\right|_{x=0^-} = -\alpha\chi_i(0). \tag{B22}$$

Scattering-state eigenfunctions satisfying $\chi_k(0^-)=\chi_k(0^+)$ and Eq. (B22) are given by

$$\chi_k = \frac{1}{\sqrt{2\pi}}\begin{cases} e^{ikx} + \dfrac{\alpha}{2ik-\alpha}e^{-ikx}, & x>0, \\ \dfrac{2ik}{2ik-\alpha}e^{ikx}, & x<0, \end{cases} \tag{B23}$$

with eigenvalue $\lambda_k^{(0)}=\delta_s^{-2}+k^2$. A single bound state satisfying these conditions also exists and is given by

$$\chi_1 \propto e^{-\alpha|x|/2}, \tag{B24}$$

with eigenvalue $\lambda_1^{(0)}=\delta_s^{-2}-(\alpha/2)^2$.

APPENDIX C: INTEGRALS FOR PREFACTOR

The integrals in Eq. (63) can be evaluated using the method of contour integration. The result is

$$\int_0^{\infty} dk \frac{\ln(k^2+\delta_s^{-2})}{k^2+\delta_s^{-2}} = \pi\delta_s \ln 2\delta_s^{-1}, \tag{C1}$$

$$\int_0^{\infty} dk \frac{\ln(k^2+\delta_s^{-2})}{k^2+\alpha^2} = \frac{\pi}{\alpha}\ln(\delta_s^{-1}+\alpha), \tag{C2}$$

and

$$\int_0^{\infty} dk \frac{(1-k^2\delta_s^2)\ln(k^2+\delta_s^{-2})}{4+8k^2\delta_s^2+\alpha^2k^2\delta_s^4+4k^4\delta_s^4} = \frac{\pi}{4\delta_s[(A^+)^2-(A^-)^2]}\left[\frac{1+(A^-)^2}{A^-}\ln(\delta_s^{-1}+\delta_s^{-1}A^-) - \frac{1+(A^+)^2}{A^+}\ln(\delta_s^{-1}+\delta_s^{-1}A^+)\right], \tag{C3}$$

where $A^{\pm}$ is given by Eq. (B19).

[1] P. Hänggi, P. Talkner, and M. Borkovec, Rev. Mod. Phys. **62**, 251 (1990).
[2] L. Néel, Ann. Geophys. (C.N.R.S.) **5**, 99 (1949).
[3] W. F. Brown, Phys. Rev. **130**, 1677 (1963).
[4] H. B. Braun, Phys. Rev. B **50**, 16501 (1994).
[5] H. B. Braun, J. Appl. Phys. **85**, 6172 (1999).
[6] P. N. Loxley and R. L. Stamps, IEEE Trans. Magn. **37**, 2098 (2001).
[7] P. N. Loxley and R. L. Stamps, Phys. Rev. B **73**, 024420 (2006).
[8] X. Wang and H. N. Bertram, J. Appl. Phys. **92**, 4560 (2002).
[9] K. A. Long and A. R. Bishop, J. Phys. A **12**, 1325 (1978).
[10] A. R. Bishop, K. Nakamura, and T. Sasada, J. Phys. C **13**, L515 (1980).
[11] K. M. Leung, J. Appl. Phys. **53**, 1858 (1982).
[12] K. M. Leung and A. R. Bishop, J. Phys. C **16**, 5893 (1983).
[13] A. M. Kosevich, B. A. Ivanov, and A. S. Kovalev, Phys. Rep. **194**, 117 (1990).
[14] H. J. Mikeska and M. Steiner, Adv. Phys. **40**, 191 (1991).
[15] W. Wernsdorfer, K. Hasselbach, A. Benoit, B. Barbara, B. Doudin, J. Meier, J. Ph. Ansermet, and D. Mailly, Phys. Rev. B **55**, 11552 (1997).
[16] A. Fert and L. Piraux, J. Magn. Magn. Mater. **200**, 338 (1999).
[17] P. M. Paulus, F. Luis, M. Kroll, G. Schmid, and L. J. de Jongh, J. Magn. Magn. Mater. **224**, 180 (2001).
[18] R. Skomski, H. Zeng, and D. J. Sellmyer, J. Magn. Magn. Mater. **249**, 175 (2002).
[19] A. Sokolov, R. Sabirianov, W. Wernsdorfer, and B. Doudin, J. Appl. Phys. **91**, 7059 (2002).
[20] H. Forster, T. Schrefl, W. Scholz, D. Suess, V. Tsiantos, and J. Fidler, J. Magn. Magn. Mater. **249**, 181 (2002).
[21] B. Hausmanns, T. P. Krome, G. Dumpich, E. F. Wassermann, D. Hinzke, U. Nowak, and K. D. Usadel, J. Magn. Magn. Mater. **240**, 297 (2002).
[22] H. Forster, N. Bertram, X. Wang, R. Dittrich, and T. Schrefl, J. Magn. Magn. Mater. **267**, 69 (2003).
[23] R. Hertel and J. Kirschner, Physica B **343**, 206 (2004).
[24] R. Wieser, U. Nowak, and K. D. Usadel, Phys. Rev. B **69**, 064401 (2004).
[25] R. Dittrich, T. Schrefl, M. Kirschner, D. Suess, G. Hrkac, F. Dorfbauer, O. Ertl, and J. Fidler, IEEE Trans. Magn. **41**, 3592 (2005).
[26] D. Suess, S. Eder, J. Lee, R. Dittrich, J. Fidler, J. W. Harrell, T.

Schrefl, G. Hrkac, M. Schabes, N. Supper, and A. Berger, Phys. Rev. B **75**, 174430 (2007).
[27] P. Bruno, Phys. Rev. Lett. **83**, 2425 (1999).
[28] J. S. Langer, Ann. Phys. **41**, 108 (1967).
[29] J. S. Langer, Ann. Phys. **54**, 258 (1969).
[30] I. V. Krive, B. A. Malomed, and A. S. Rozhavsky, Phys. Rev. B **42**, 273 (1990).
[31] T. Christen, Phys. Rev. E **51**, 604 (1995).
[32] R. Skomski and J. M. Coey, *Permanent Magnetism* (IOP, Bristol, 1999).
[33] H. B. Braun, Phys. Rev. B **50**, 16485 (1994).
[34] R. Giachetti, P. Sodano, E. Sorace, and V. Tognetti, Phys. Rev. B **30**, 4014 (1984).
[35] P. Sodano, M. El-Batanouny, and C. R. Willis, Phys. Rev. B **34**, 4936 (1986).
[36] G. Barton, J. Phys. A **18**, 479 (1985).
[37] A. Seeger and P. Schiller, in *Physical Acoustics*, edited by W. P. Mason (Academic, New York, 1966), Vol. 3, p. 361.
[38] J. F. Currie, J. A. Krumhansl, A. R. Bishop, and S. E. Trullinger, Phys. Rev. B **22**, 477 (1980).
[39] K. M. Leung, Phys. Rev. B **26**, 226 (1982).
[40] R. Pathria, *Statistical Mechanics*, 2nd ed. (Elsevier, New York, 1996), p. 96.
[41] S. Coleman, in *The Whys of Subnuclear Physics*, edited by A. Zichichi (Plenum, New York, 1979).
[42] L. S. Schulman, *Techniques and Applications of Path Integration* (Wiley, New York, 1981), pp. 271–289.
[43] J. Rubinstein, J. Math. Phys. **11**, 258 (1970).